A vacancy-interstitial defect pair model for positive-bias temperature stress-induced electron trapping transformation in the high-κ gate n-MOSFET

Gu, Chenjie; Ang, Diing Shenp; Gao, Yuan; Gu, Renyuan; Zhao, Ziqi; Zhu, Chao

2017

Gu, C., Ang, D. S., Gao, Y., Gu, R., Zhao, Z., & Zhu, C. (2017). A vacancy-interstitial defect pair model for positive-bias temperature stress-induced electron trapping transformation in the high-κ gate n-MOSFET. IEEE Transactions on Electron Devices, 64(6), 2505-2511.

https://hdl.handle.net/10356/86839

https://doi.org/10.1109/TED.2017.2694440

A Vacancy-Interstitial Defect Pair Model for Positive-Bias Temperature Stress-Induced Electron Trapping Transformation in the High-κ Gate n-MOSFET

Chenjie Gu, Diing Shenp Ang, Yuan Gao, Renyuan Gu, Ziqi Zhao, and Chao Zhu

***Abstract*— Recent device reliability studies have observed the shallow-to-deep transformation of electron-trap states under positive-bias temperature stressing. Being two typical types of defects in the high-κ oxide, the oxygen vacancy and oxygen interstitial have been investigated in many simulations, but results have indicated that the corresponding defect levels are either too shallow or too deep and fail to explain the experimental observation. Here, we propose a vacancy-interstitial (V_O-O_i) model. By tuning the relative positions of V_O and O_i, we show that the charge trap level of the defect pair can be adjusted continuously within the HfO_2 bandgap. This allows us to depict a possible atomic picture for understanding the shallow-to-deep transformation of electron trapping.**

***Index Terms*— CMOS reliability, dynamic bias temperature instability (BTI), high-κ dielectric, oxide traps, V_O-O_i defect pair.**

I. Introduction

THE replacement of the polysilicon/oxynitride gate-stack by the metal/high-κ gate-stack is one of the most significant moves made by the semiconductor industry. Although the latter has enabled the further downscaling of equivalent oxide thickness (EOT) and suppression of gate leakage current [1]–[3], it has also brought along a new set of challenges [4]–[6]. Among these, the bias temperature instability (BTI) is believed to be an extremely critical one, which manifests itself as time-dependent drifts of key performance parameters such as threshold voltage, drain current, *etc*. [7], [8]. While negative-BTI (NBTI) was already a serious concern for the polysilicon/oxynitride gate p-MOSFET [9] before the changeover was made, the metal/high-κ gate-stack suffers from an additional positive-BTI (PBTI) problem, which severely impacts the performance of the n-MOSFET [10], [11]. Therefore, there has been considerable effort made in recent years to understand the underlying mechanisms governing the BTI issues in the metal/high-κ gate-stack [12]–[16].

To-date, a good level of consistency has been attained in terms of the experimental behaviors of the BTI problem. Broadly, BTI induced parametric shift may be divided into two parts: 1) a recoverable part typically characterized by a rapid relaxation transient that sets in upon removal of the applied stress and 2) a relatively permanent part that builds up steadily over time and accounts for the long-term parametric shift. In early studies on NBTI, these two parts were assumed to originate from different mechanisms [17], [18]. Recent works [19] have, however, consistently revealed a link between them, whereby part of the recoverable portion may be transformed into a more permanent form as the stressing continues. More recent studies on small-area transistors have unambiguously demonstrated such a recoverable-to-permanent transformation behavior of individual oxide trap [20], [21]. Meanwhile, atomistic simulation studies have provided a microscopic picture of the degradation mechanism [22], [23]. In [24], a discussion on the vacancy-interstitial (V_O-O_i) defect pair reveals its capability to act as either a shallow or deep trap level, depending on the specific V_O-O_i structure. However, knowledge on the defect pair dynamics and the corresponding electrical behaviors under stress is still not available.

In this paper, we observe, through continuous defect structure relaxation, that the electron-trap state of a V_O-O_i defect pair could vary across the entire bandgap of HfO_2, depending on the relative positions of V_O and O_i. This allows us to conclude that the V_O-O_i defect pair is a promising candidate for the shallow-to-deep electron-trap state transformation observed during PBTI testing.

Manuscript received January 5, 2017; revised March 6, 2017 and March 27, 2017; accepted April 11, 2017. The review of this paper was arranged by Editor R. M. Todi. This work was supported in part by the Singapore Ministry of Education Research under Grant MOE2013-T2-2-099 and MOE2016-T2-1-102, in part by the K. C. Wong Magna Fund in Ningbo University, and in part by the open funding of the first-class disciplines in physics, Zhejiang Province under Grant 008-421600972. *(Corresponding author: Chenjie Gu.)*

C. Gu, Z. Zhao, and C. Zhu are with the Division of Microelectronics Science and Engineering, School of Science, Ningbo University, Ningbo 315211, China (e-mail: guchenjie@nbu.edu.cn).

D. S. Ang is with the School of Electrical and Electronic Engineering, Nanyang Technological University, Singapore 639798 (e-mail: edsang@ntu.edu.sg).

Y. Gao is with Micron Semiconductor Asia Pte Ltd, Singapore 339942.

R. Gu is with the School of Computer Science and Information Security, Guilin University of Electronic Technology, Guilin 541004, China.

Color versions of one or more of the figures in this paper are available online at http://ieeexplore.ieee.org.

Digital Object Identifier 10.1109/TED.2017.2694440

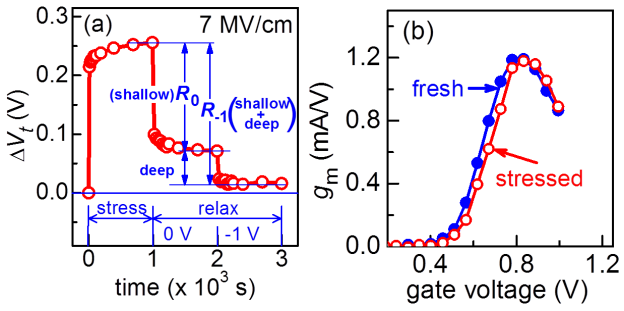

Fig. 1. (a) Evolution of threshold voltage shift ΔV_t during PBTI stressing followed by relaxation. Initial oxide stress field was 7 MV/cm, [estimated based on $(V_g - V_{t0})$/EOT, where V_g is gate stress voltage and V_{t0} is prestress threshold voltage]; relaxation was carried out at $V_g = 0$ V for 1×10^3 s, followed by -1 V for another 1×10^3 s. The temperature was 100 °C. (b) Compared with the prestress transconductance curve, the curve after PBTI stress is laterally shifted toward more positive V_g without reduction in the peak value. This test device was stressed with a 1-MHz V_g pulse alternating between +1.9 V (~7 MV/cm) and 0 V for 5×10^3 s.

II. Shallow-to-Deep Electron-Trap State Transformation

In this section, we review recent experimental results showing the transformation of electron trapping from shallow-to-deep energy levels during PBTI stressing [25].

A. Deep-Level Electron Trapping

The test devices were n-MOSFETs with 0.25- and 10 − μm drawn channel length and width, respectively. The gate-stack consisted of a 3-nm atomic-layer-deposited HfO_2 and a 0.9-nm SiO_x interfacial layer, with an EOT of 1.4 nm. Fig. 1 shows the threshold voltage shift (ΔV_t) in a typical PBTI stress/relax cycle obtained through the ultrafast-switching method [26]. The relaxation curve shows that besides the shallow-level electron trapping responsible for the fast recovery transient [27], a nonnegligible ΔV_t stems from electrons trapped at deep energy states. This is evident from the second abrupt decrease of ΔV_t that occurred during the -1 V recovery, applied upon the prior 0 V recovery reaching a quasi-saturation level. Since a negative gate voltage (V_g) will further bring down the Fermi level toward the Si valence band, the second abrupt ΔV_t decrease may be ascribed to the emission of electrons trapped at deeper energy states in the HfO_2 bandgap. After the -1 V recovery, the remnant ΔV_t is ~0, which implies that the electrons trapped in deep energy states were almost fully detrapped, i.e., nearly the entire ΔV_t was due to electron trapping. This is also apparent in another test device, whose transconductance curve is shifted laterally toward more positive V_g after PBTI stress, without any apparent decrease in the peak value [Fig. 2(b)], indicating that electron trapping is the dominant degradation mechanism for PBTI [28].

B. Conversion of Shallow-to-Deep-Level Electron Trapping

As can be seen from the ΔV_t evolution in a single stress/relax cycle [Fig. 1(a)], PBTI stress leads to electron trapping in a broad range of trap states in the HfO_2 bandgap. For a given relax interval, electrons trapped at relatively

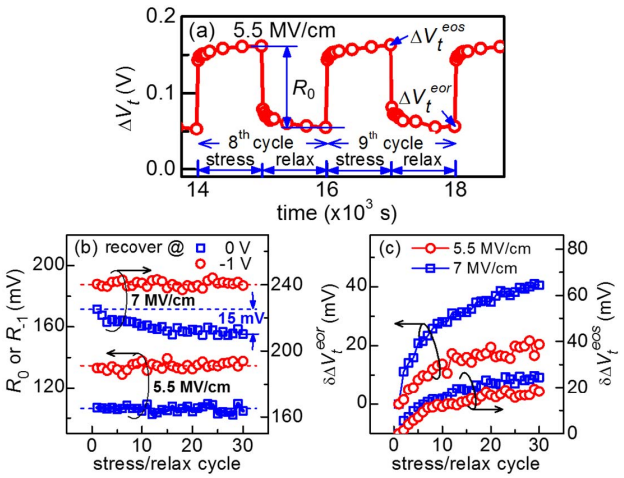

Fig. 2. (a) Evolution of ΔV_t under alternate PBTI stress (5.5-MV/cm oxide field at the beginning of PBTI cycle) and 0 V relaxation over selected stress/relax cycles. (b) ΔV_t recovery per 0 V (R_0) or -1 V (R_{-1}) relaxation interval as a function of the number of stress/relax cycles applied. (c) $\delta\Delta V_t^{eos} = \Delta V_t^{eos}(n^{th}\text{ cycle}) - \Delta V_t^{eos}(1^{st}\text{ cycle})$ (right axis) and $\delta\Delta V_t^{eor} = \Delta V_t^{eor}(n^{th}\text{ cycle}) - \Delta V_t^{eor}(1^{st})$ (left axis) as a function of the number of stress/relax cycles applied for the case of 0 V relaxation.

shallow-level states are able to emit, whereas those trapped at deeper states can be emitted only with the aid of a negative V_g. These deep states may include those originally deep ones generated by the stress or shallow ones, which were converted quickly into deeper ones when the stress was applied (i.e., the conversion time constants are much shorter than the stress interval). To differentiate the part of deep-level electron trapping which results from shallow-level traps having longer time constants, multiple stress/relax cycles are needed. The conversion of these shallow-level traps may be inferred from the decrease of R_0 (Fig. 2) as explained in the following [19].

Fig. 2(a) shows typical ΔV_t change over selected cycles, for a device stressed at an oxide field of 5.5 MV/cm [1] and relaxed at 0 V. The ΔV_t recovery per relax cycle, denoted as R_0, is approximately constant, independent of the number of stress/relax cycles [Fig. 2(b)]. As R_0 results from the emission of electrons at relatively shallow trap states [see Fig. 1(a)], a constant R_0 means that the number of electron emissions from shallow trap states is nearly fixed in each relax interval. This is reasonable, since these shallow trap states would be readily refilled in the next stress interval, and emissions from the same group of shallow trap states would then occur in the following relax interval. A similar result is obtained on another test device stressed under the same condition but relaxed at -1 V. Here, the ΔV_t recovery per relax cycle (denoted as R_{-1}) is increased, because additional electron emissions from deeper trap states are possible under -1 V relaxation [see Fig. 1(a)]. On the other hand, the evolution of R_0 is different for a device stressed at a higher oxide field of 7 MV/cm. A steady decrease of R_0 can be observed, indicating that the number of electron emissions from shallow trap states is gradually reduced as more stress/relax cycles were applied. However, such a decrease is not observed for R_{-1}, which

[1] Oxide field here refers in particular to the oxide field at the beginning of the PBTI cycle, the same definition is used for the rest of this paper.

remains nearly constant as in the case of the 5.5-MV/cm stress.

Fig. 2(c), wherein the evolution of ΔV_t^{eos} and ΔV_t^{eor} (with respect to the first cycle) is compared, offers an insight into the progressive decrease of R_0 seen at the higher 7-MV/cm stress. ΔV_t^{eos}, taken at the end of each stress interval [Fig. 2(a)], reflects the total electron trapping prior to the start of relaxation. On the other hand, ΔV_t^{eor}, taken at the end of each relax interval, gives the remnant electron trapping, i.e., electrons trapped at deep energy states and were unable to emit during the relax interval. Under the 5.5-MV/cm stress, the steady increase of ΔV_t^{eos} means that in each stress interval, besides the retrapping of electrons at shallow trap states "emptied" in the previous relax interval, there was additional trapping of electrons at deep trap states. The similar rise in ΔV_t^{eor} implies that these trapped electrons were unable to emit at the end of the following relax cycle, resulting in a gradual accumulation of deep-level electron trapping. For the 7-MV/cm stress, ΔV_t^{eos} increases at a similar rate as that of the 5.5 MV/cm, indicating that the incremental electron trapping at deep trap states after each stress interval is comparable under both oxide stress fields. However, ΔV_t^{eor} increases at a faster rate than that of the 5.5-MV/cm stress. This means that at the end of each relax interval, the remnant electron trapping, i.e., electrons trapped at deep energy states, increases more quickly under the 7-MV/cm stress. Given that the incremental electron trapping at deep trap states per stress interval is similar for both oxide stress fields, the results thus imply that the gradual reduction in R_0 under the 7-MV/cm stress is due to some of the formerly shallow trap states being transformed into deeper ones as stressing is continuously applied. We speculate that such transformation may involve the transition from a metastable shallow trap state to a deeper trap state [29], facilitated by oxide-field-induced lowering of the energy barrier.

To check the above-mentioned conclusion, stressing was carried out under the same oxide stress field of 7 MV/cm but with a relaxation voltage of -1 V. Since electron emissions from deep trap states can also occur, the decrease in R_0 or emissions from shallow trap states (due to the conversion of some of these states to deeper levels) seen under the 0 V relaxation should be suppressed under the -1 V relaxation. This is because even if a shallow trap state has changed into a deeper one, emission from the resultant trap state may still occur under the -1 V relaxation [see Fig. 1(a)]. This inference is indeed borne out by the evolution of R_{-1} [Fig. 2(c)]. Other than the expected increase in R_{-1} over R_0, the reduction in R_0 is not observed in R_{-1}. The nearly constant R_{-1} result supports our conclusion that the decrease in R_0 stems from shallow-to-deep trap state transformation.

III. Defect Model and Simulation Method

The relatively high density of defects in low-temperature deposited high-κ oxides (as compared with the thermally grown SiO_2) has attracted considerable attention. Electron spin resonance studies on high-κ oxides have shown the existence of both oxygen vacancy (V_O) and oxygen interstitial (O_i) defects [30]. *Ab-initio* simulation has found that the electron-trap state associated with V_O is rather shallow ($\sim 1\ eV$ below the HfO_2 conduction band edge), whereas that linked to O_i is very deep (near to the valence band edge) [31]. Therefore, neither V_O nor O_i is able to explain the above experimental phenomenon. In view that high-κ oxides are generally oxygen deficient, the presence of O_i alone is unlikely. Moreover, being transition metal oxides, the metal–oxygen bonds have a partial ionic character. In HfO_2, the $Hf-O$ bond has $\sim$70% ionic character [32]. Under an applied electric field, weak $Hf-O$ bonds in the amorphous oxide may tend to break. In view of the above-mentioned considerations, the presence of O_i near a V_O is a likely scenario. Therefore, in the following simulation work, we focus on the V_O-O_i defect pair; evolution of the defect level with a change in the relative positions of V_O and O_i is investigated in detail.

First principles simulation was performed by Vienna *Ab initio* Simulation Package [33]–[36], which employed the plane wave pseudopotential methods within the density functional theory [37]. The ultrasoft pseudopotential was used to represent the interactions between the ion core and the valence electrons. The exchange correlation energies were treated within the generalized gradient approximation of Perdew *et al.* [38]. In all calculations, the cutoff energy and points were tested. For structure optimization, the conjugate gradient method was used and the ion positions were optimized until the residual force was less than 0.01 eV/Å. The hybrid scheme was used here to correct the bandgap so that the trap level could be precisely determined [39]. The formation energy E_f of a defect in HfO_2 was calculated from the total energy E of the defective supercell per the following formula [40]:

$$E_f(\alpha, q) = E(\alpha, q) - (E_0^0 + n_{Hf}\mu_{Hf} + n_0\mu_0) + q(\epsilon_F + E_{\text{VBM}}) \quad (1)$$

where E_0^0 is the system energy of the defect-free supercell and E_{VBM} is the valence band maximum of HfO_2. For a defect α in charge state q, E_f is a function of the Fermi level ϵ_F and the respective chemical potential of Hf and O denoted by μ_{Hf} and μ_O. The terms n_{Hf} and n_O represent the corresponding number of Hf and O atom(s) added/removed from the supercell to form the defect. The charge transition level (CTL) for negative-to-neutral ($-/0$) state transition of the defect is also calculated and is given by ϵ_F, which corresponds to $E_f(\alpha, q) = 0$. The $-/0$ CTL, measured with respect to E_{VBM}, is akin to the trap level of the defect in the HfO_2 bandgap [41]. The supercell used in our simulation study was amorphous HfO_2, which was generated from a crystalline HfO_2, via molecular dynamics, following the melt-and-quench scheme [42]. It consisted of 48 Hf atoms and 96 O atoms, with a density of 9.68 g/cm^3.

To introduce a V_O-O_i defect pair into the amorphous HfO_2 supercell, a lattice oxygen atom (O_L) was manually moved to a nearby lattice vacancy position (Fig. 3). However, as this initial structure might be energetically unfavorable, it was subjected to full structure relaxation under a negative charged environment until the structure reached the stable state ($S0$). In subsequent study on the V_O-O_i defect pair, we fixed the

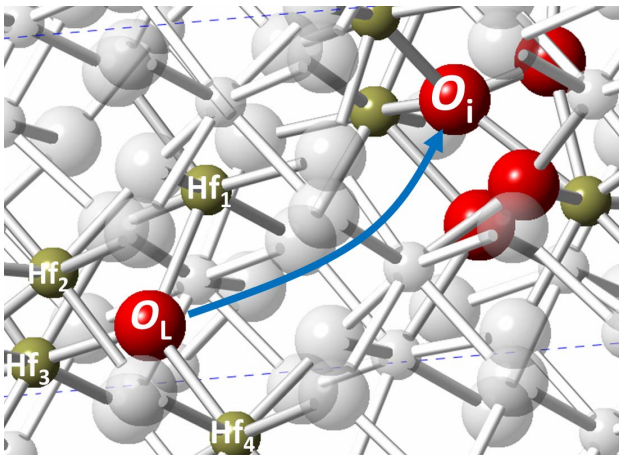

Fig. 3. V_O-O_i defect is created by moving the lattice oxygen (O_L) to a neighboring lattice vacancy (O_i). This initial structure was then subjected to fully structure relaxation until it reached the stable state ($S0$).

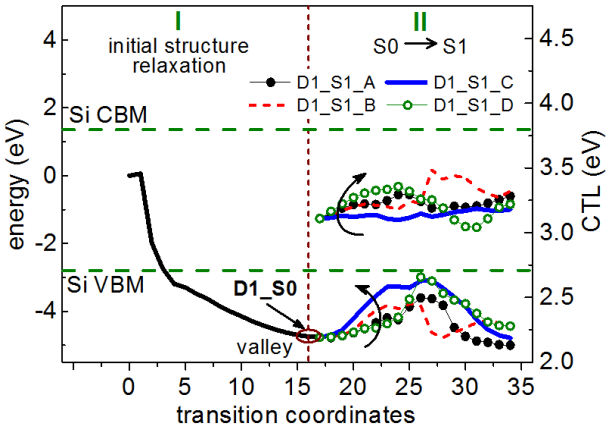

Fig. 4. Change in system energy along the MEP for (I) initial structural relaxation toward a stable state S_0, following the creation of a V_O-O_i defect pair (D_1) by manual relocation of a lattice oxygen atom to a nearby lattice vacancy position. (II) Further evolution of $D1\_S0$ toward four new stable defect structures ($D1\_S0\_A$, $D1\_S0\_B$, $D1\_S1\_C$, and $D1\_S1\_D$), via O_i relocation along four possible paths to other nearby lattice vacancies. Change in the charge trap level is also shown.

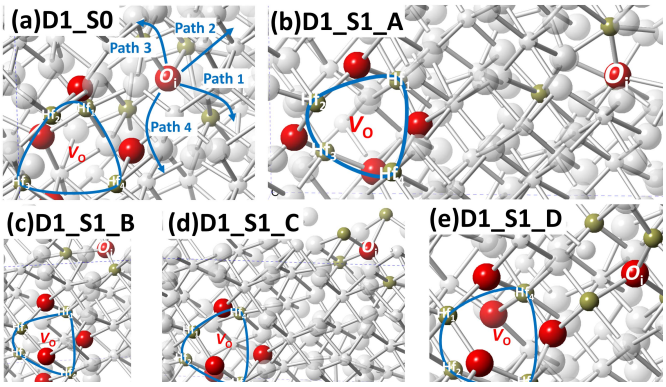

Fig. 5. (a) Atomic structure of the D1 defect (Fig. 3) following full structural relaxation ($D1\_S0$). Arrows show four possible paths along which O_i may migrate to a new lattice vacancy position, leading to a further evolution of $D1\_S0$. Stable defect structures obtained after O_i has migrated to a new lattice vacancy along paths 1–4 are denoted as (b) $D1\_S1\_A$, (c) $D1\_S1\_B$, (d) $D1\_S1\_C$, and (e) $D1\_S1\_D$, respectively.

position of V_O and moved the O_i to the other neighboring lattice vacancy positions, thus changing the relative positions of V_O and O_i. Structure relaxation was performed after each O_i position change until the new structure reached a stable state. The minimum energy path (MEP) for the transformation between the consecutive two defect structures was calculated by the nudged elastic band method [43]. Meanwhile, the CTL change during the defect transformation process was extracted.

We investigated a total of ten V_O-O_i defect pairs based on the amorphous HfO_2 supercell. Here, we discuss two cases showing characteristics that support the shallow-level electron trapping and shallow-to-deep defect transformation phenomenon evidenced in our experimental work. The other cases show either stable switching or fixed charging characteristics, and will be discussed elsewhere.

IV. Simulation Results Discussion

We give a full picture of the MEP and CTL results pertaining to the evolution of the first V_O-O_i defect pair ($D1$) in Fig. 4. As aforementioned, the V_O-O_i defect was generated by moving one O_L to an arbitrary lattice vacancy position. It was not a stable defect initially. This is evident in the phase I of Fig. 4, which shows a steep drop in the system energy during the structural relaxation step. After this, the supercell with the $D1$ defect reached a stable state and is named $D1\_S0$ [Fig. 5(a)]. As guided by the arrows on Fig. 5(a), there are four possible paths (1–4) along which O_i may migrate to get to a new position, one lattice vacancy away from V_O. Therefore, we manually moved the O_i to each of the four lattice vacancies, thus creating four new defect structures. These four structures were then subjected to structural relaxation until they each reached a final stable state ($S1$). The resultant defect structures, $D1\_S1\_A$, $D1\_S1\_B$, $D1\_S1\_C$, and $D1\_S1\_D$, corresponding to O_i migration along paths 1–4, are shown in Fig. 5(b)–(e), respectively. The MEP and CTL (for a total of 18 intermediate atomic structures or transition coordinates) were also calculated for each of the four models, and the results are shown in the phase II of Fig. 4. From MEP results, the energy barriers E_B for the transformation from $S0$ to each of the four $S1$ states (A, B, C, and D) is 1.16, 1, 1.77, and 1.68 eV, respectively. At temperature $T = 100$ °C, the corresponding time constant τ ($=\tau_0 \cdot \exp(E_B/\kappa T)$; $\tau_0 = 10^{-13}$ s; κ is Boltzmann's constant [44]) for the transformation are ~470, 3, 8×10^{10}, and 5×10^3 s. Thus, upon the application of stress, $D1\_S0$ may readily be transformed into $D1\_S1\_B$. The CTL of $D1\_S0$ is ~3.1 eV, near the middle of the Si bandgap, which shows that $D0\_S1$ is a shallow electron-trap state. After the transformation, the CTL is relatively unchanged (in fact it becomes slightly shallower). $D1\_S1\_B$ remains a shallow electron-trap state and the transformation is not detectable from the ΔV_t relaxation characteristic.

Results for the second V_O-O_i defect pair ($D2$) are shown in Figs. 6 and 7. The first step of structure relaxation brought it to a more stable state ($D2\_S0$), as manifested by the decrease in system energy (phase I of Fig. 6). The CTL of $D2\_S0$ is ~ 3.4 eV, which is also around the middle of the silicon

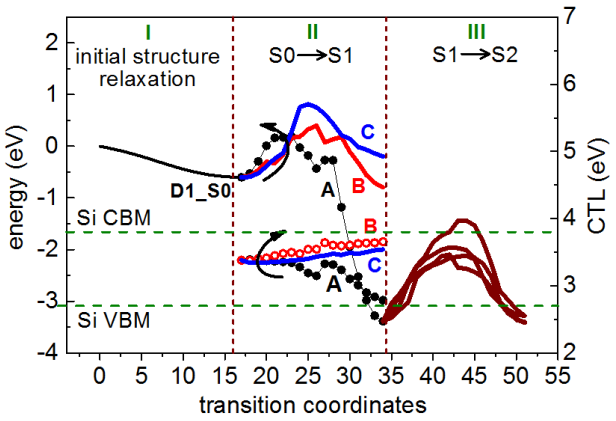

Fig. 6. Change in system energy along the MEP for (I) initial structural relaxation of a V_O-O_i defect pair $D2$ toward a stable state $S0$. (II) Further evolution of $D2\_S0$ toward three new stable defect structures ($D2\_S1\_A$, $D2\_S1\_B$, and $D2\_S1\_C$), via O_i relocation along three possible paths to other nearby lattice vacancies. Change in the charge trap level is also shown. (III) Further evolution of $D2\_S1\_A$ to other new stable structures by O_i migration along four possible pathways.

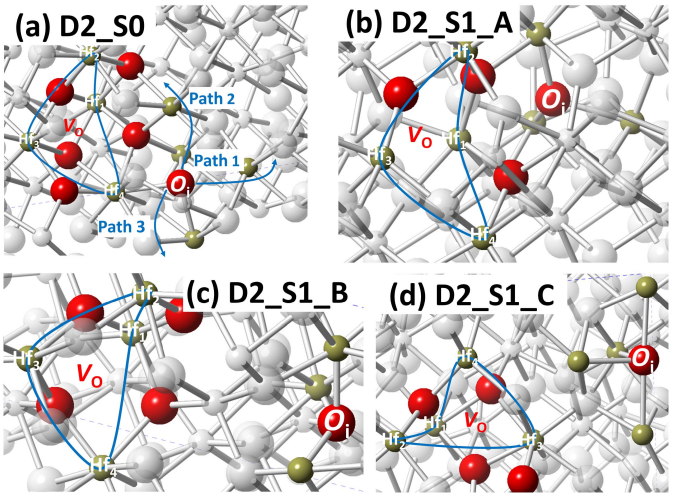

Fig. 7. (a) Atomic structure of a V_O-O_i defect pair $D2$ in a stable state following an initial structural relaxation. (b)–(d) New stable defect structures could evolve from $D2\_S0$, via O_i migration along three possible paths [1–3, respectively, as shown in (a)] to other nearby lattice vacancies.

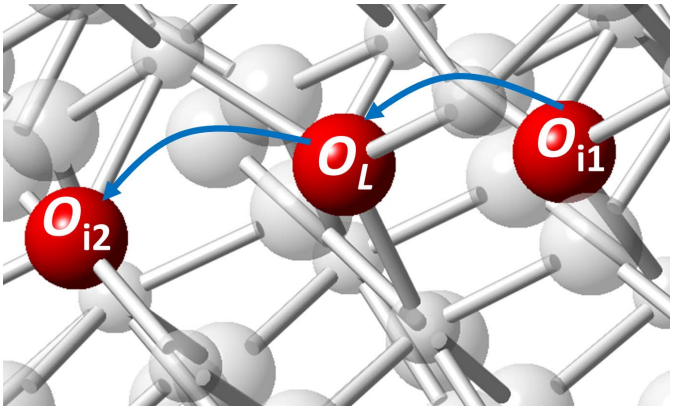

Fig. 8. Illustration of how an interstitial oxygen of a V_O-O_i defect pair migrates to a nearby lattice vacancy position inside the HfO_2 network. O_{i1} represents the initial position of the oxygen interstitial, O_L is a nearby lattice oxygen, and O_{i2} is the destination lattice vacancy. The migration proceeds with O_{i1} moving toward O_L and O_L moving toward the destination lattice vacancy position. Finally, O_{i1} replaces O_L, with O_L being relocated to O_{i2}.

gap. Like $D1\_S0$, $D2\_S0$ is also a shallow electron-trap state. A check on the surrounding of the $D2\_S0$ structure [Fig. 7(a)] shows three available migration paths (1–3) for O_i to get to a new neighboring lattice vacancy. Thus, we manually created three defect structures by moving O_i along each of the paths. All three defect structures were then subjected to structure relaxation until each reached a final stable state ($S1$). The resultant defect structures, $D2\_S1\_A$, $D2\_S1\_B$, and $D2\_S1\_C$, corresponding to O_i migration along path $1-3$, are shown in Fig. 7(b)–(d), respectively. The MEP as well as the CTL results for the three evolution cases is shown in phase II of Fig. 6. We find that for $D2\_S1\_A$, the transformation energy barrier is 0.877 eV, lower than those of the other two cases; 1 eV for $D2\_S1\_B$ and 1.41 eV for $D2\_A1\_C$. More importantly, the evolution of $D2\_S0$ to $D2\_S1\_A$ is accompanied by a much larger decrease in system energy as compared with the other two cases. These results imply that the O_i migration would occur preferentially along path 1. With the help of the increased local electric field due to the applied stress, O_i may overcome the energy barrier and then relocates itself by migrating along path 1 to the new lattice vacancy. In the process, the CTL is decreased from the middle of the Si bandgap toward the valence band edge, representing a change from a shallow to a deeper electron-trap state (phase II, Fig. 6). This finding provides a strong support for the shallow-to-deep level electron-trapping transformation inferred experimentally (Fig. 2). Though the rather small τ of 70 ms suggests that the transformation of $D2\_S0$ should readily occur in a short stress period, time constants comparable or much longer than the stress interval used in this paper may be expected considering the amorphous network of HfO_2.

We have also checked the possibility of a further evolution of $D2\_S1\_A$ by calculating the energy barriers for O_i migration from its present position to other neighboring lattice vacancies along four possible pathways, denoted as $S1 \rightarrow S2$ transition phase (III) in Fig. 6. The minimum energy barrier is 1.28 eV, which corresponds to a τ of 1.9×10^4 s, much longer than the stress interval of 1×10^3 s. Moreover, there is no lowering of the system energy in the $S2$ state. It is also worth mentioning that the energy barrier for the change from $D2\_S1\_A$ back to $D2\_S0$ is rather large ($\sim$3.8 eV). These findings imply that $D2\_S1\_A$ would tend to remain in the local "energy valley" of its current state and is not likely to revert to $D2\_S0$ even under a moderate negative V_g or further transformed under stressing for fixed stress and relax intervals. This relative stability of $D2\_S1\_A$ as a deep electron-trap state may explain why even under $V_g = -1$ V relaxation, a progressive increase of ΔV_t^{eor} with stress/relaxation cycling can still be observed (not shown), indicating a gradual build-up of deep-level electron trapping, although the rate of increase is lesser than the case of $0 - V$ relaxation (Fig. 2).

We have also examined the trajectory of O_i during the migration process. It is found that O_i moves by a "swapping" method, as shown in Fig. 8 and elaborated in the following. O_{i1} represents the initial position of the interstitial oxygen

of a V_O-O_i defect pair. With the help of the local electric field or high temperature, O_{i1} moves toward a lattice oxygen denoted as O_L. Meanwhile, O_L moves away from its original lattice position toward the destination lattice vacancy position, labeled as O_{i2}. In the end, O_{i1} takes the place of O_L, with O_L being relocated to O_{i2}. Through this swapping method, the migration of O_i can occur throughout the whole HfO_2 network.

V. Conclusion

Experimental results from PBTI stress/relaxation cycling have indicated that electron trapping may change from an initial shallow trap state to a deeper trap state. Here, we present a V_O-O_i defect pair model, which may satisfactorily explain such a transformation. It is found that a V_O-O_i defect pair may evolve into a much more stable state, with the O_i migrating from its original location to a different lattice vacancy position, as marked by a substantial decrease in the system energy at the end of the O_i migration process. This evolution is shown in some cases to correspond to a shift in the electron-trap state to a deeper energy level. This atomic model could explain not only the shallow-to-deep electron-trap state transformation, but also long-term PBTI recovery involving the reverse transformation of an electron-trap state from a deep to a shallower level with the concurrent emission of the trapped electron. This paper provides a possible atomic picture of the underlying mechanisms governing the dynamics of the PBTI reliability issue in high-κ/metal gate-stacks.

References

[1] E. Gusev, D. A. Buchanan, E. Cartier, and A. Kumar, "Ultrathin high-*k* gate stacks for advanced CMOS devices," in *IEDM Tech. Dig.*, Dec. 2001, pp. 20.1.1–20.1.4.

[2] R. M. Wallace and G. D. Wilk, "High-κ dielectric materials for microelectronics," *Critical Rev. Solid State Mater. Sci.*, vol. 28, no. 4, pp. 231–285, Oct. 2003.

[3] T. P. Ma, "Electrical characterization of high-*k* gate dielectrics," in *Proc. ICSSICT*, Oct. 2004, pp. 361–365.

[4] A. S. Oates, "Reliability issues for high-*k* gate dielectrics," in *IEDM Tech. Dig.*, Dec. 2003, pp. 38.2.1–38.2.4.

[5] E. Cartier, B. P. Linder, V. Narayanan, and V. K. Paruchuri, "Fundamental understanding and optimization of PBTI in nFETs with SiO_2/HfO_2 gate stack," in *IEDM Tech. Dig.*, Dec. 2006, pp. 1–4.

[6] K. Onishi *et al.*, "Reliability characteristics, including NBTI, of polysilicon gate HfO_2 MOSFETs," in *IEDM Tech. Dig.*, Feb. 2011, pp. 30.3.1–30.3.4.

[7] N. Kimizuka, T. Yamamoto, T. Mogami, K. Yamaguchi, K. Imai, and T. Horiuchi, "The impact of bias temperature instability for direct-tunneling ultra-thin gate oxide on MOSFET scaling," in *Symp. VLSI Technol. Dig. Tech. Papers*, Jun. 1999, pp. 73–74.

[8] Y. Mitani, M. Nagamine, H. Satake, and A. Toriumi, "NBTI mechanism in ultra-thin gate dielectric–nitrogen-originated mechanism in SiON," in *IEDM Tech. Dig.*, Dec. 2002, pp. 509–511.

[9] V. Huard, M. Denais, and C. Parthasarathy, "NBTI degradation: From physical mechanisms to modelling," *Microelectron. Rel.*, vol. 46, no. 1, pp. 1–23, Jan. 2006.

[10] G. Bersuker *et al.*, "Mechanism of electron trapping and characteristics of traps in HfO_2 gate stacks," *IEEE Trans. Device Mater. Reliab.*, vol. 7, no. 1, pp. 138–145, Mar. 2007.

[11] Y. Gao, D. S. Ang, and C. J. Gu, "On the evolution of switching oxide traps in the HfO_2/TiN gate stack subjected to positive- and negative-bias temperature stressing," *ECS Trans.*, vol. 53, no. 3, pp. 205–220, May 2013.

[12] L. Vandelli, L. Larcher, D. Veksler, A. Padovani, G. Bersuker, and K. Matthews, "A charge-trapping model for the fast component of positive bias temperature instability (PBTI) in high-κ gate-stacks," *IEEE Trans. Electron Devices*, vol. 61, no. 7, pp. 2287–2293, Jul. 2014.

[13] S. Mukhopadhyay and S. Mahapatra, "An experimental perspective of trap generation under BTI stress," *IEEE Trans. Electron Devices*, vol. 62, no. 7, pp. 2092–2097, Jul. 2015.

[14] G. Rzepa, M. Waltl, W. Goes, B. Kaczer, and T. Grasser, "Microscopic oxide defects causing BTI, RTN, and SILC on high-*k* FinFETs," in *Proc. SISPAD*, Sep. 2015, pp. 144–147.

[15] A. Ranjan *et al.*, "CAFM based spectroscopy of stress-induced defects in HfO_2 with experimental evidence of the clustering model and metastable vacancy defect state," in *Proc. IEEE Int. Reliab. Phys. Symp. (IRPS)*, Apr. 2016, pp. 7A-4–7A-7A–4–7.

[16] T. Grasser *et al.*, "The 'permanent' component of NBTI revisited: Saturation, degradation-reversal, and annealing," in *Proc. IEEE Int. Reliab. Phys. Symp. (IRPS)*, Apr. 2016, pp. 5A-2–5A-5A–2–8.

[17] S. Mahapatra *et al.*, "A comparative study of different physics-based NBTI models," *IEEE Trans. Electron Devices*, vol. 60, no. 3, pp. 901–916, Mar. 2013.

[18] T. Grasser, K. Rott, H. Reisinger, M. Waltl, F. Schanovsky, and B. Kaczer, "NBTI in nanoscale MOSFETs–The ultimate modeling benchmark," *IEEE Trans. Electron Devices*, vol. 61, no. 11, pp. 3586–3593, Nov. 2014.

[19] Y. Gao, A. A. Boo, Z. Q. Teo, and D. S. Ang, "On the evolution of the recoverable component of the SiON, HfSiON and HfO_2 P-MOSFETs under dynamic NBTI," in *Proc. IEEE Int. Reliab. Phys. Symp. (IRPS)*, Apr. 2011, pp. 935–940.

[20] J. Franco *et al.*, "Impact of single charged gate oxide defects on the performance and scaling of nanoscaled FETs," in *Proc. IEEE Int. Reliab. Phys. Symp. (IRPS)*, Apr. 2012, pp. 5A4.1–5A4.6.

[21] Z. Y. Tung and D. S. Ang, "Impact of voltage-accelerated stress on hole trapping at operating condition," *IEEE Electron Device Lett.*, vol. 37, no. 5, pp. 644–647, May 2016.

[22] R. öttking *et al.*, "Defect generation and activation processes in HfO_2 thin films: Contributions to stress-induced leakage currents," *Phys. Status Solidi A*, vol. 212, no. 3, pp. 547–553, Mar. 2015.

[23] Y. Wimmer, A.-M. El-Sayed, W. Gös, T. Grasser, and A. L. Shluger, "Role of hydrogen in volatile behaviour of defects in SiO_2-based electronic devices," *Proc. R. Soc. Lond. A, Math. Phys. Sci.*, vol. 472, no. 2190, pp. 1364–5021, Jun. 2016.

[24] D. S. Ang, C. J. Gu, Z. Y. Tung, A. A. Boo, and Y. Gao, "Evolution of oxide charge trapping under bias temperature stressing," *Microelectron. Reliab.*, vol. 54, no. 4, pp. 663–681, Apr. 2014.

[25] Y. Gao, D. S. Ang, G. Bersuker, and C. D. Young, "Electron trap transformation under positive-bias temperature stressing," *IEEE Electron Device Lett.*, vol. 34, no. 3, pp. 351–353, Mar. 2013.

[26] G. A. Du, D. S. Ang, Z. Q. Teo, and Y. Z. Hu, "Ultrafast measurement on NBTI," *IEEE Electron Device Lett.*, vol. 30, no. 3, pp. 275–277, Mar. 2009.

[27] M. Ershov *et al.*, "Dynamic recovery of negative bias temperature instability in *p*-type metal–oxide–semiconductor field-effect transistors," *Appl. Phys. Lett.*, vol. 83, no. 8, pp. 1647–1649, Aug. 2003.

[28] S. Pae *et al.*, "BTI reliability of 45 nm high-k + metal-gate process technology," in *Proc. IEEE Int. Reliab. Phys. Symp. (IRPS)*, Apr./May 2008, pp. 352–357.

[29] T. Grasser, B. Kaczer, H. Reisinger, P. J. Wagner, and M. Toledano-Luque, "On the frequency dependence of the bias temperature instability," in *Proc. IEEE Int. Reliab. Phys. Symp. (IRPS)*, Apr. 2012, pp. XT.81–XT.87.

[30] J. P. Campbell, P. M. Lenahan, C. J. Cochrane, A. T. Krishnan, and S. Krishnan, "Atomic-scale defects involved in the negative-bias temperature instability," *IEEE Trans. Device Mater. Rel.*, vol. 7, no. 4, pp. 540–557, Dec. 2007.

[31] K. Xiong and J. Robertson, "Point defects in HfO_2 high *k* gate oxide," *Microelectron. Eng.*, vol. 80, pp. 408–411, Jun. 2005.

[32] A. Y. Kang, P. M. Lenahan, and J. F. Conley, "Electron spin resonance observation of trapped electron centers in atomic-layer-deposited hafnium oxide on Si," *Appl. Phys. Lett.*, vol. 83, no. 16, pp. 3407–3409, Oct. 2003.

[33] G. Kresse and J. Hafner, "Ab initio molecular dynamics for liquid metals," *Phys. Rev. B, Condens. Matter*, vol. 47, no. 1, pp. 558–561, Jan. 1993.

[34] G. Kresse and J. Hafner, "*Ab initio* molecular-dynamics simulation of the liquid metal amorphous semiconductor transition in germanium," *Phys. Rev. B, Condens. Matter*, vol. 49, no. 20, p. 14251–14269, May 1994.

[35] G. Kresse and J. Furthmüller, "Efficiency of ab-initio total energy calculations for metals and semiconductors using a plane-wave basis set," *Comput. Mater. Sci.*, vol. 6, pp. 15–50, Jul. 1996.

[36] G. Kresse and J. Furthmüller, "Efficient iterative schemes for ab initio total-energy calculations using a plane-wave basis set," *Phys. Rev. B, Condens. Matter*, vol. 54, no. 16, p. 11169–11186, Oct. 1996.
[37] D. Vanderbilt, "Soft self-consistent pseudopotentials in a generalized eigenvalue formalism," *Phys. Rev. B, Condens. Matter*, vol. 41, no. 11, p. 7892, Apr. 1990.
[38] J. P. Perdew, K. Burke, and M. Ernzerhof, "Generalized gradient approximation made simple," *Phys. Rev. Lett.*, vol. 77, pp. 3865–3868, Oct. 1996.
[39] P. Broqvist, A. Alkauskas, and A. Pasquarello, "A hybrid functional scheme for defect levels and band alignments at semiconductor–oxide interfaces," *Phys. Status Solidi A*, vol. 207, no. 2, pp. 270–276, Feb. 2010.
[40] C. G. Van de Walle and J. Neugebauer, "First-principles calculations for defects and impurities: Applications to III-nitrides," *J. Appl. Phys.*, vol. 95, no. 8, pp. 3851–3879, 2004.
[41] A. Alkauskas, P. Broqvist, and A. Pasquarello, "Defect energy levels in density functional calculations: Alignment and band gap problem," *Phys. Rev. Lett.*, vol. 101, no. 4, pp. 046405-1–046405-4, Jul. 2008.
[42] W. Scopel, A. Da Silva, and A. Fazzio, "Amorphous HfO_2 and $Hf_{1-x}Si_xO$ via a melt-and-quench scheme using *ab* initio molecular dynamics," *Phys. Rev. B, Condens. Matter*, vol. 77, no. 17, p. 172101, May 2008.
[43] G. Henkelman and H. Jónsson, "A climbing image nudged elastic band method for finding saddle points and minimum energy paths," *J. Chem. Phys.*, vol. 113, no. 22, pp. 9901–9904, Nov. 2000.
[44] K. S. Ralls *et al.*, "Discrete resistance switching in submicrometer silicon inversion layers: Individual interface traps and low-frequency ($\frac{1}{f}$) noise," *Phys. Rev. Lett.*, vol. 52, no. 3, pp. 228–231, Jan. 1984.

Authors' photographs and biographies not available at the time of publication.